Influence of Li ions on memristor properties of capacitor structures based on nanocomposites $(Co_{40}Fe_{40}B_{20})_x(LiNbO_3)_{100-x}$

© A.V. Sitnikov,[1,2] Yu.E. Kalinin,[1] I.V. Babkina,[1] A.E. Nikonov,[1] M.N. Kopytin,[1] L.I. Yanchenko,[1] A.R. Shakurov[1]

[1] Voronezh State Technical University,
394026 Voronezh, Russia
[2] National Research Center „Kurchatov Institute",
123182 Moscow, Russia
e-mail: Aleks.shakurov@mail.ru

The paper reveals the influence of Li, B and the composition of metal contacts on the processes of resistive switching in memristive structures M/NC/D/M. After field exposure in structures $Cu/(Co_{50}Fe_{50})_x(LiNbO_3)_{100-x}$/s-LiNbO$_3$/Cu/sitall, $Cu/(Co_{50}Fe_{50})_x(LiNbO_3)_{100-x}$/d-LiNbO$_3$/Cu/sitall and $Cu/(Co_{40}Fe_{40}B_{20})_x(SiO_2)_{100-x}$/d LiNbO$_3$/Cu/sitall at $x < 13$ was detected a residual voltage (up to 16 mV) due to the electromigration of Li ions, that leading to a "reversible" type of VAC hysteresis and instability of the time dependencies of induced resistive states. In the structures of $Cu/(Co_{40}Fe_{40}B_{20})_x(LiNbO_3)_{100-x}$/s-LiNbO$_3$/Cu/sitall, $Cr/Cu/Cr/(Co_{40}Fe_{40}B_{20})_x(LiNbO_3)_{100-x}$/s-LiNbO$_3$/Cr/Cu/Cr/sitall containing B, the residual voltage is reduced by formation of chemical compounds B with percolated Li atoms. When limiting the electromigration of Li ions, the main mechanism of resistive switching is the processes of electromigration of oxygen vacancies in the dielectric oxide layer. Suppression of residual voltage in the $Cr/Cu/Cr/(Co_{50}Fe_{50})_x(LiNbO_3)_{100-x}$/s-LiNbO$_3$/Cr/Cu/Cr/sitall structure due to the introduction of a Cr buffer layer that does not dissolve Li leads to the absence of bipolar resistive switching in these structures.

Keywords: Resistive switching, memristive effect, nanocomposite, residual voltage, thin-films structures.

Introduction

At present, research on the creation of neuromorphic electronic systems that simulate the functions of the human brain, such as the ability to learn, pattern recognition, natural language, etc. [1–6] is of great interest. The most promising elements in a neuromorphic network are memristors that model the action of synapses and are capable of quasi-continuously and reversibly changing and maintaining their electrical resistance in a certain range of values.

The main mechanisms of resistive switching (RS) in memristive structures are usually associated with the processes of electromigration of oxygen vacancies in the dielectric oxide layer or metal cations (type Cu, Ag) into the dielectric from the active electrode (containing cation atoms) of the metal/dielectric/metal (MDM) [1,7–9] structure. As a result of these processes, filamentary conductive channels (filaments) [7] are formed (destroyed) in the dielectric layer. The spatial formation of filaments is a largely random event and is usually associated with defects in the memristor structure (oxygen vacancies) [7]. This is one of the main reasons for the degradation of memristor properties under cyclic RP [7,8].

The authors managed to solve the problem of degradation of memristor properties during cyclic resistive switching by using nanocomposite (NC) as one of the electrodes. Conductive channels of contiguous metal pellets were formed, which set the surface concentration and spatial arrangement of the filaments formed in the dielectric interlayer. Thus, for metal/NK/metal (M/NK/M) structures based on NCs $(Co_{40}Fe_{40}B_{20})_x(LiNbO_3)_{100-x}$, a resistive switching effect was observed with the value of the ratio of high-resistive to low-resistive states $Roff/Ron \approx 100$, which was well reproduced at the number of RP cycles $> 10^5$ [10–13]. As shown by the studies, the main reason for the presence of RP in the composite $(Co_{40}Fe_{40}B_{20})_x(LiNbO_3)_{100-x}$ is the formation of an amorphous dielectric interlayer of $10-15$ nm LiNbO$_3$ thickness at the initial stage of nanocomposite growth on the bottom metal electrode by the self-organization process [14,15]. Therefore, it is more correct in terms of functional characteristics to represent the structure $M/(Co_{40}Fe_{40}B_{20})_x(LiNbO_3)_{100-x}$/M as $M/(Co_{40}Fe_{40}B_{20})_x(LiNbO_3)_{100-x}$/s-LiNbO$_3$/M, where s-LiNbO$_3$ — dielectric layer obtained as a result of self-organization processes (s — self-organized). In addition, boron atoms are uniformly distributed in both the metallic and dielectric phases of the nanocomposite [14]. It is clear that the presence of Li and B in the functional

layers of M/NK/M memristive structures cannot but influence RP processes. Therefore, the main objective of the present work was to establish the regularities of the influence of these atoms on the memristive characteristics of $M/(Co_{40}Fe_{40}B_{20})_x(LiNbO_3)_{100-x}/LiNbO_3/M$ capacitor structures.

1. Samples and study methods

M/NK/D/M memristive structures were prepared by ion-beam sputtering, where heterogeneous films $(Co_{40}Fe_{40}B_{20})_x(LiNbO_3)_{100-x}$, $(Co_{50}Fe_{50})_x(LiNbO_3)_{100-x}$ served as NCs and $(Co_{40}Fe_{40}B_{20})_x(SiO_2)_{100-x}$ (hereinafter for brevity we will denote these composites, as $(CoFeB)_x(LiNbO_3)_{100-x}$, $(CoFe)_x(LiNbO_3)_{100-x}$ and $(CoFeB)_x(SiO_2)_{100-x}$ respectively), and as a dielectric layer (D) — interlayers of s-LiNbO₃ formed by self-organization during NC deposition, or a d-LiNbO₃ film (d — deposition) deposited from a target consisting of a plate of single-crystalline LiNbO₃. Cr-Cu (M) films or Cr-Cu-Cr (M1) or Cr-Cu-Cr (M3) three-layer conductors were used as metal electrode (M) layers. The composition and structure of the studied systems are presented in Fig. 1 and in the table.

Three process operations of ion-beam sputtering were used to obtain the memristive structures. In the first step, a metal coating, which is either a Cu film or a Cr-Cu-Cr multilayer structure, was deposited on the cital substrates. Prior to sputtering, ion cleaning of the substrate surface was performed, then the wafers were moved to the sputtering Cr target position, where a chromium metal film with a thickness of ~ 100 nm was deposited for 10 min. Then, using a rotationally controlled substrate holder, the samples were moved to the Cu deposition zone from the corresponding target, where a copper film with a thickness of ~ 1000 nm for 30 min was deposited, followed by a repeat of the Cu deposition operation (~ 100 nm for 10 min). When sputtering Cu contact, the first and last operation of deposition of layer M was skipped.

The functionalized layer was synthesized in one deposition cycle. For this purpose, the sitalloy substrates were arranged in a row of 4 plates. The sample for sputtering had a surface 240×48 mm. The substrates were covered with a shadow screen with 8 mm diameter holes arranged in 24 rows of 6 holes per row. Films of D and NK layers were deposited through this mask. In samples of series 5 and 6, the LiNbO₃ interlayer was synthesized from the original single-crystal lithium niobate target of $280 \times 80 \times 2$ mm. Synthesis was performed on the rotating substrate as it passed through the deposition zone. At a

Figure 1. Topology of the experimental samples M/NK/D/M/M.

Structure of M/NK/D/M memristors

№ bottom	Metal top contact	HK	D	Metal sample contact
1	Cr-Cu-Cr	$(CoFeB)_x(LiNbO_3)_{100-x}$	s-LiNbO₃	Cr-Cu-Cr
2	Cu	$(CoFeB)_x(LiNbO_3)_{100-x}$	s-LiNbO₃	Cu
3	Cr-Cu-Cr	$(CoFe)_x(LiNbO_3)_{100-x}$	s-LiNbO₃	Cr-Cu-Cr
4	Cu	$(CoFe)_x(LiNbO_3)_{100-x}$	s-LiNbO₃	Cu
5	Cu	$(CoFe)_x(LiNbO_3)_{100-x}$	d-LiNbO₃	Cu
6	Cu	$(CoFeB)_x(SiO_2)_{100-x}$	d-LiNbO₃	Cu

rotation speed of 0.2 rpm, a discharge current of 100 mA, and an anode voltage of 2 kV, a film with a thickness of ~ 5 nm was synthesized in one pass. Three passes of the substrates in the dielectric sputtering zone were used in the technological process. The synthesis was carried out in an Ar atmosphere ($P_{Ar} \approx 3.9 \cdot 10^{-4}$ Torr) with the addition of oxygen ($P_{O_2} \approx 1.9 \cdot 10^{-5}$ Torr).

The NC layer was deposited from a composite target with a non-uniform arrangement of dielectric suspensions, which allowed a smooth and continuous change in the concentration of the composite metal phase on the substrate surface depending on the substrate-target [16,17] arrangement. During the synthesis of the NK layer, oxygen was added to the working gas atmosphere ($P_{Ar} \approx 3.9 \cdot 10^{-4}$ Torr) at a pressure of $P_{O_2} \approx 0.9 \cdot 10^{-5}$ Torr. A film with a thickness of ≈ 250 nm was formed during a sputtering time of 15 min. The variation of metal phase concentration in the composite was from 5 to 23 at.%.

Top contact pads made of Cu or Cr-Cu-Cr multilayer structure were applied through a metal mask with hole size $0.5 - 0.2$ mm using the technique described above.

It should be noted that the vacuum ion-beam sputtering unit has an oil-free pumping system. The pre-vacuum was less than $1 \cdot 10^{-6}$ Torr. Particularly pure gases of at least 99.999% were used for sputtering. Prior to sputtering, the target surface was dusted and the substrates were ion cleaned.

The elemental composition of NCs was determined using an Oxford INCA Energy 250 energy-dispersive X-ray attachment on a JEOL JSM-6380 LV scanning election microscope. The accuracy of determining the composition of the samples was determined by their size, discrete location on the substrates and was $x \pm 1$ at.%.

The current-voltage curve (CVC) of M/NK/D/M structures and their memristive properties were measured using a KEITHLEY 2450 multifunctional source-measuring device and an analytical probe station in current-limited mode. The magnitude of residual voltage was recorded with a universal voltmeter V7-78/1. The CVC of the M/NK/D/M structures were measured with the bottom electrode grounded and the bias voltage U sweep of the top electrode following
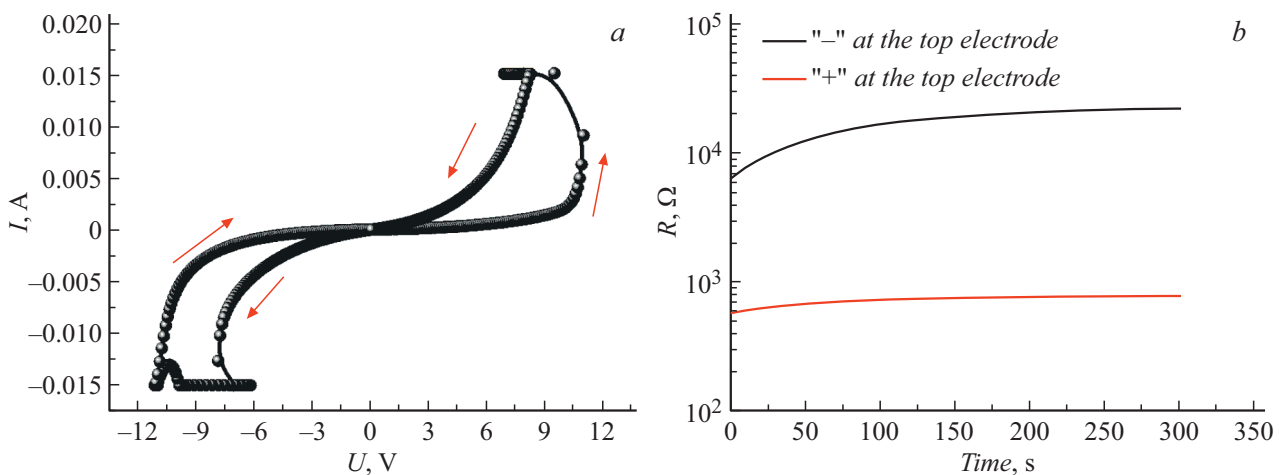
Figure 2. BAX (*a*) and time dependence of induced resistive states (*b*) of M3/(CoFeB)$_{8.5}$(LiNbO$_3$)$_{91.5}$/s-LiNbO$_3$/M3. memristive structures.

a linear law in the sequence from $0 | +U_{max} | -U_{max} | 0$ V with pitch 0.1 V. The rate of voltage change was 10 V/s. The temporal stability of the induced resistive state was measured after CVC measurement at a reading voltage of 0.1 V. The residual voltage on the structures (U_{res}) was recorded after field exposure at the optimum (with respect to breakdown current and absence of CVC relaxation) current limitation of 60 s duration for a given structure. The time interval after field exposure and residual stress fixation was $\sim$ 10 s. Before measurements U_{res} contacts were shorted to each other.

2. Results and discussion

The typical CVC and time stability of the induced resistive state for the M3/(CoFeB)$_x$(LiNbO$_3$)$_{100-x}$/s-LiNbO$_3$/M3 (№1 in the table) memristive structures are shown in Fig. 2. It can be seen that the RP from R_{off} to R_{on} occurs at positive and the reverse RP from R_{on} to R_{off} — at negative bias at the top electrode. Moreover, the induced resistive states are quite stable. When the contact material is changed from M3 to M1, the CVC dependence does not change fundamentally (Fig. 3, *a*). But if we remove boron from the composite, the dependencies change fundamentally. We do not observe switching to the high-resistance state of the structure at the negative bias at the top electrode (Fig. 3, *b*). Changing the contact material from M3 to M1 in the structures with composite CoFe)$_x$(d-LiNbO$_3$)$_{100-x}$ „flips" the dependence, and we observe a transition to the high-resistance state at positive bias at the top electrode (Fig. 3, c). The use of d-LiNbO$_3$ instead of s-LiNbO$_3$ in such structures does not fundamentally change the course of the CVC (Fig. 3, *d*). If instead of the nanocomposite (CoFeB)$_x$(LiNbO$_3$)$_{100-x}$ a film of the heterogeneous system(CoFeB)$_x$(SiO$_2$)$_{100-x}$, is used, then at low concentrations of the metallic phase we observe a dependence similar to that for the M3/(CoFe)$_{8.5}$(LiNbO$_3$)$_{91.5}$/s-LiNbO$_3$/M3

structure (Fig. 3, *e*), and at large x, we observe an inverse CVC (Fig. 3, *f*).

This diversity of characteristics must have a physical justification. By taking a close look at the composition and topology of the structures under study, we can identify the elements that make up lithium-ion batteries [18]. They require Li atoms, a medium in which Li ions can travel, and two reservoirs where lithium can accumulate. From this point of view, consider the structure M1/(CoFe)$_x$(LiNbO$_3$)$_{100-x}$/s-LiNbO$_3$/M1. The source of Li atoms can be either the s-LiNbO$_3$ interlayer, or the dielectric matrix of the nanocomposite (CoFe)$_x$(LiNbO$_3$)$_{100-x}$. The medium where ionic current is possible is amorphous lithium niobate. It is found that single-crystalline LiNbO$_3$ is a very poor ionic conductor at room temperature with lithium diffusion activation energy of the order of 1.4 eV [19]. At the same time, lithium niobate in the amorphous state has a diffusion constant Li by $\sim$ 8 orders of magnitude greater than in the single-crystal, and the activation energy of the diffusion process $\sim$ 0.7 eV, which is quite sufficient to consider this medium as an ionic conductor [19]. Lithium has limited solubility in Cu up to 13 at.% at room temperature [20], low diffusion constant, which can be divided into lattice ($D_0 = 3.9 \cdot 10^{-9}$ cm^2/s; $E_a = 0.68$ eV) and grain boundary ($D_0 = 1.5 \cdot 10^{-11}$ cm^2/s; $E_a = 0.36$ eV) [21]. However, in many cases, an abnormally high diffusion activity Li was observed in the near-surface 3 − 5 nm layer of the copper electrode, which was attributed to the increased concentration of surface defects [22]. In our case, the ion cleaning process prior to sputtering the functional layers is a process that introduces additional defects into the near-surface layer of the metal contact. Based on this, it can be assumed that the copper electrode in the investigated systems can act as a reservoir of Li atoms. In addition, Co is incorporated into the metallic phase of the composite. The film of the latter is synthesized by ion-beam sputtering in Ar atmosphere with the addition of O$_2$.
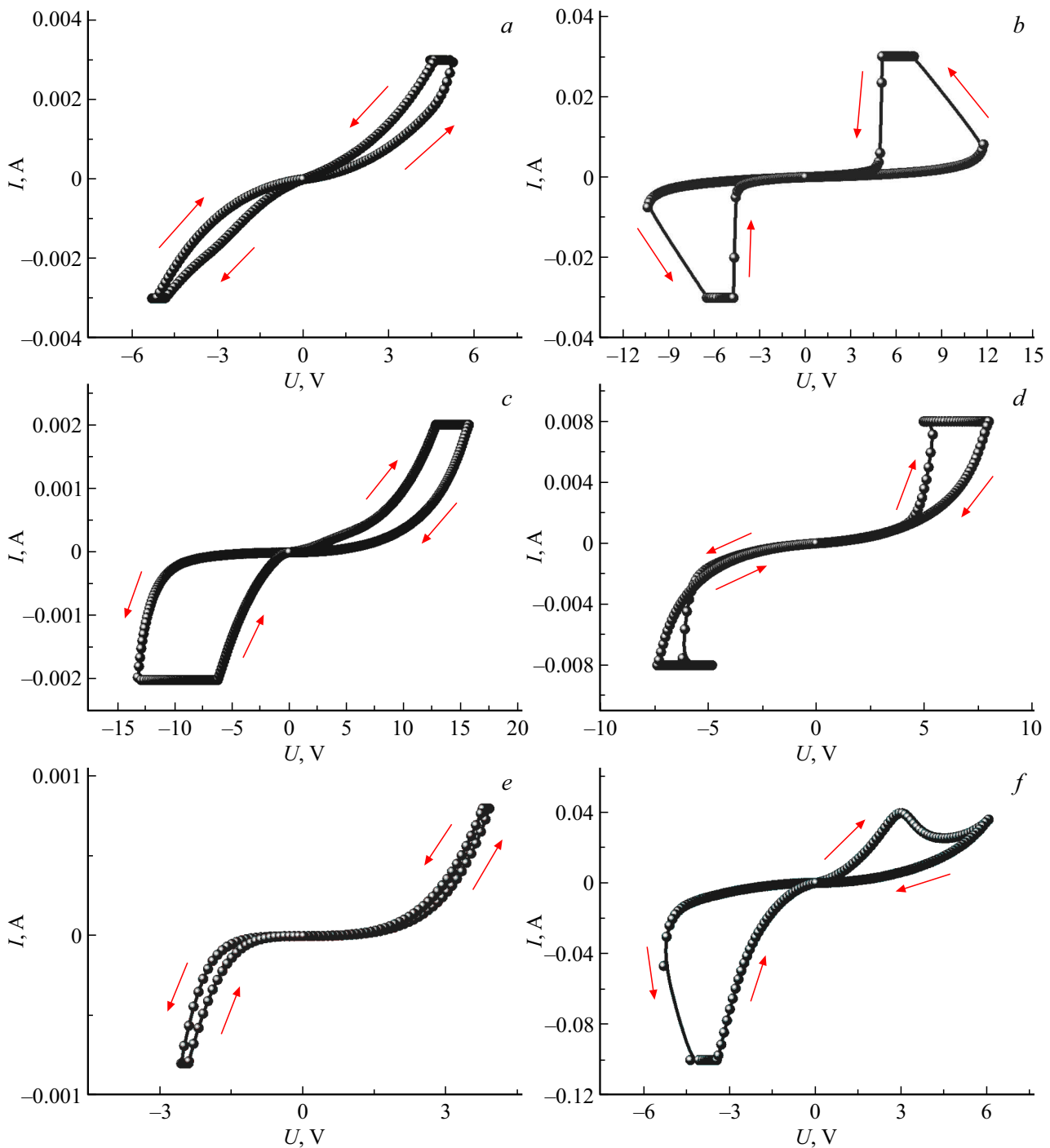
Figure 3. CVC of memristive structures: a — M1/(CoFeB)$_{8.5}$(LiNbO$_3$)$_{91.5}$/s-LiNbO$_3$/M1, b — M3/(CoFe)$_{8.5}$(LiNbO$_3$)$_{91.5}$/s-LiNbO$_3$/M3, c — M1/(CoFe)$_{8.5}$(LiNbO$_3$)$_{91.5}$/s-LiNbO$_3$/M1, d — M1/(CoFe)$_{8.5}$(LiNbO$_3$)$_{91.5}$/d-LiNbO$_3$/M1, e — M1/(CoFeB)$_{8.5}$(SiO$_2$)$_{91.5}$/d-LiNbO$_3$/M1, f — M1/(CoFeB)$_{13.7}$(SiO$_2$)$_{84.3}$/d-LiNbO$_3$/M1.

Consequently, some of the cobalt may be in an oxidized state. Cobalt oxide and the LiCoO$_2$ compound formed from it are the standard storage reservoir for lithium ions in lithium-ion batteries.

To reveal the ability of the studied structures to accumulate electric charge, the samples were subjected to field exposure for 60 s, and then the time depen-

dences of the induced voltage were recorded. As an example, the characteristic dependences for the structure M1/(CoFe)$_{8.5}$(LiNbO$_3$)$_{91.5}$/s-LiNbO$_3$/M1 (CVC of Fig. 3, c), are shown in Fig. 4.

Even though ~ 10 s passes after the charging process and before the residual voltage (U$_{res}$) is measured and the contacts are short-circuited during this time interval,
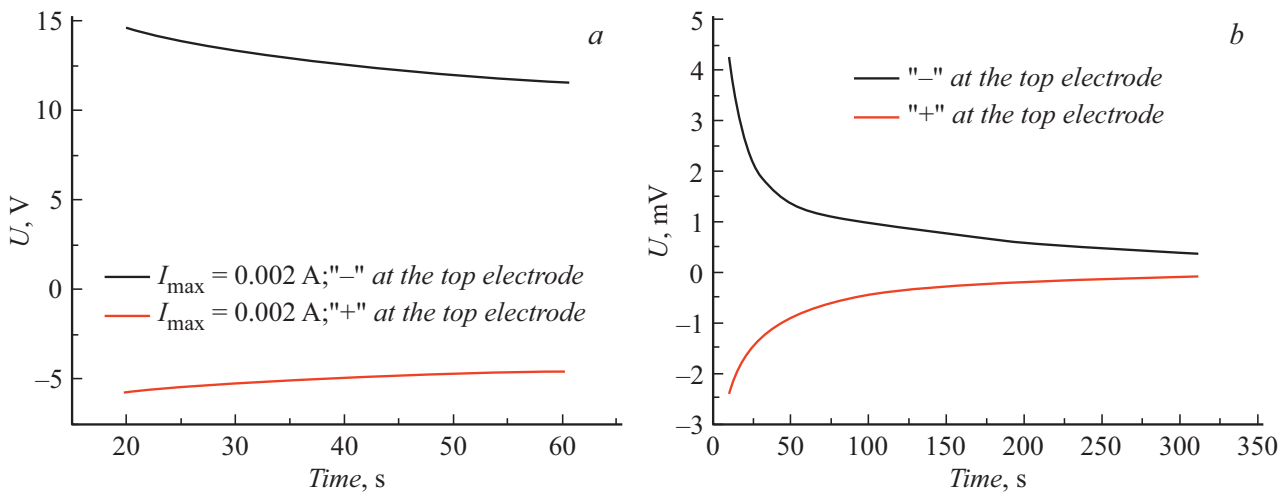
Figure 4. Time dependences of field exposure (*a*) and residual stress after field exposure (*b*) on the structure M1/$(CoFe)_{8.5}(LiNbO_3)_{91.5}$/s-LiNbO$_3$/M1.
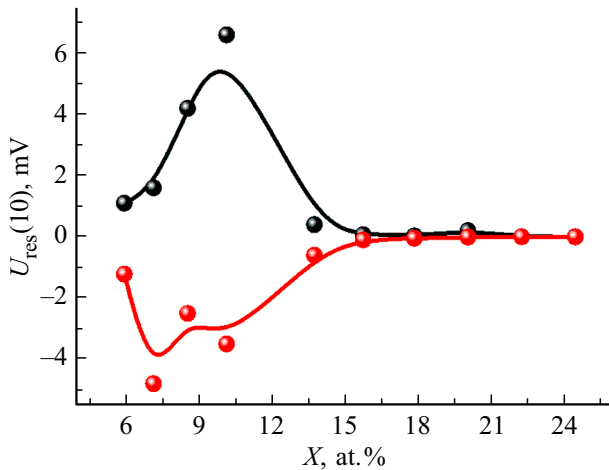
Figure 5. Concentration dependences of residual stress in 10 s after field impact on the structure M1/$(CoFe)_x(LiNbO_3)_{100-x}$/s-LiNbO$_3$/M1.

we record a rather high value of $U_{res}(t) \sim mV$, which persists between a few mV and 100 s. To evaluate the presence and magnitude of the residual stress effect in the studied structures, the value of $U_{res}(t)$ was chosen as a criterion in 10 s after field exposure of the sample, further — $U_{res}(10)$. A typical concentration curve for the structures M1/$(CoFe)_x(LiNbO_3)_{100-x}$/s-LiNbO$_3$/M1 is presented in Fig. 5, from which it can be seen that in the whole concentration range up to the percolation threshold of nanocomposites$(CoFe)_x(LiNbO_3)_{100-x}$ ($x < 15$ at.%) a rather high value of $U_{res}(10)$ of the order of several mV is recorded, which confirms our assumptions about significant electromigration of Li ions in the investigated structures.

Fig. 6 shows the values of $U_{res}(10)$ for the structures whose CVCs are shown in Figs. 2 and 3.

Analysis of the obtained results shows that the highest values of $U_{res}(10)$ are observed in the structures where Cu is used as an electrical contact in the LiNbO$_3$ interlayer (Fig. 6, positions *4−6*) and the metal phase of the composite does not contain boron (Fig. 6, positions *4, 5*). In this case, the way of organizing the LiNbO$_3$ interlayer (s or d) does not play an essential role. If a Cr buffer layer is added to the structure, $U_{res}(10)$ is significantly suppressed (Fig. 6, positions *3* and *1*). Indeed, Cr does not dissolve Li jcite20 and one of the reservoirs of lithium accumulation disappears. The boron effect on the residual stress is most interesting. We see that in structures where the composite includes B, the value of $U_{res}(10)$ is significantly smaller than
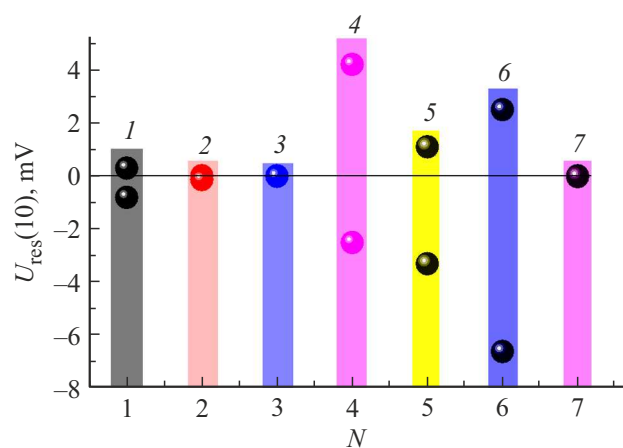
Figure 6. Residual stress 10 s after the field effect on the structure: *1* — M3/$(CoFeB)_{8.5}(LiNbO_3)_{91.5}$/s-LiNbO$_3$/M3, *2* — M1/$(CoFeB)_{8.5}(LiNbO_3)_{91.5}$/ s-LiNbO$_3$/M1, *3* — M3/$(CoFe)_{8.5}(LiNbO_3)_{91.5}$/s-LiNbO$_3$/M3, *4* — M1/$(CoFe)_{8.5}(LiNbO_3)_{91.5}$/s-LiNbO$_3$/M1, *5* — M1/$(CoFe)_{8.5}(LiNbO_3)_{91.5}$/d-LiNbO$_3$/M1, *6* — M1/$(CoFeB)_{8.5}(SiO_2)_{91.5}$/d-LiNbO$_3$/M1, *7* — M1/$(CoFeB)_{13.7}(SiO_2)_{84.3}$/d-LiNbO$_3$/M1.
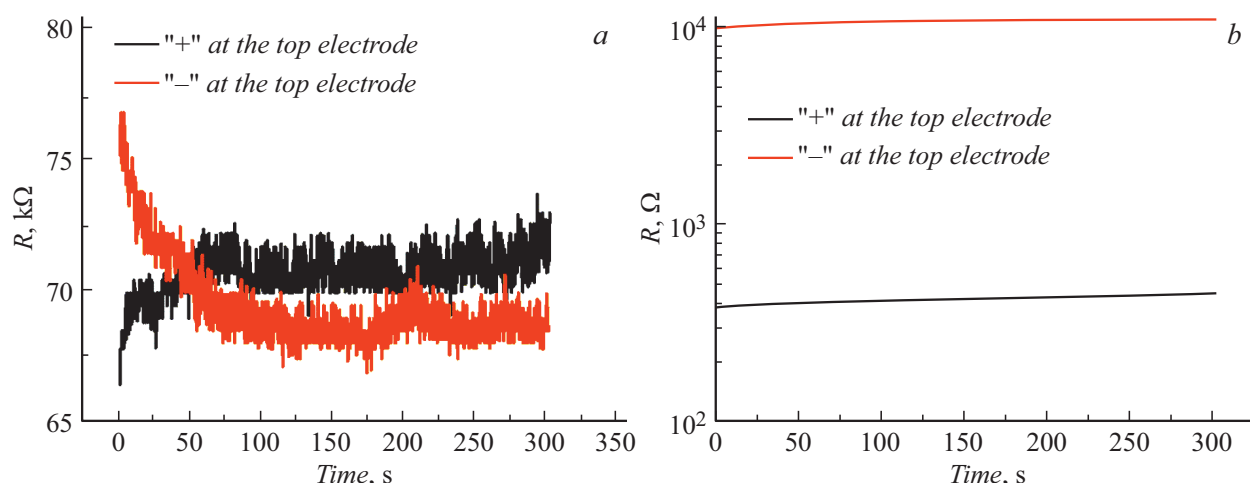
Figure 7. Time dependences of induced resistive states of the structures: a — M1/(CoFe)$_{8.5}$(LiNbO$_3$)$_{91.5}$/s-LiNbO$_3$/M1, b — M1/(CoFeB)$_{13.7}$(SiO$_2$)$_{84.3}$/d-LiNbO$_3$/M1.

in its absence (cf. Fig. 7, positions *2* and *4*). As we noted above [20], our studies of the structure and phase composition of (CoFeB)$_x$(LiNbO$_3$)$_{100-x}$ composites showed that up to 50% of boron atoms are dissolved in the dielectric matrix. On the other hand, boron and lithium can form a range of chemical compounds B$_4$Li, B$_{12}$Li, B$_4$Li$_5$, B$_6$Li$_7$, BLi$_3$, B$_{14}$Li$_3$, B$_6$Li, B$_{19}$Li$_6$, B$_3$Li, B$_2$Li and BLi. It can be hypothesized that boron atoms in the dielectric matrix of the nanocomposite and dielectric interlayer can act as effective traps of percolated lithium atoms involved in ionic conduction. The structure M1/(CoFeB)$_x$(SiO$_2$)$_{100-x}$/d-LiNbO$_3$/M1,where the presence of B atoms in the composite does not suppress U$_{res}$. It can be assumed that dissolved boron atoms in amorphous SiO$_2$ bind to the dielectric matrix to form a borosilicate glass type compound and are not able to act as effective traps for diffusing lithium atoms.

We now compare the obtained results for U$_{res}$ and their interpretation with the CVCs of the investigated systems. In systems where boron suppressed U$_{res}$ due to chemical interaction with Li atoms, a CVC hysteresis associated with electromigration of oxygen vacancies is observed (Figs. 2 and 3, *a*). Where U$_{res}$ is suppressed by the introduction of the barrier layer Cr, we do not capture bipolar resistive switching (Fig. 3, *b*). In the presence of high U$_{res}$ values, bipolar resistive switching is observed, but it has a „reversed" appearance relative to normal switching (Fig. 3, *c*−*e*). In addition, the time dependences of the induced resistive states are extremely unstable in this case (Fig. 7), for example, in the case where U$_{res}$ becomes negligible at high concentrations of the metallic phase in the system M1/(CoFeB)$_x$(SiO$_2$)$_{100-x}$/d-LiNbO$_3$/M1 (Fig. 6, position 7). The reversed character of the CVC can be observed (Fig. 3, *f*), but the induced resistive states are quite stable (Fig. 7, *b*), and the switching occurs most likely due to the electromigration process of Cu cations.

Conclusion

The studies presented in this work have shown that the presence of Li and B atoms in the functional layers of M/NK/D/M memristive structures, as well as the composition of metal contacts have a significant effect on the resistive switching processes. So, in the structures M1/(CoFe)$_x$(LiNbO$_3$)$_{100-x}$/s-LiNbO$_3$/M1, M1/(CoFe)$_x$(LiNbO$_3$)$_{100-x}$/d-LiNbO$_3$/M1, M1/(CoFeB)$_x$(SiO$_2$)$_{100-x}$/d-LiNbO$_3$/M1 at $x < 13$ at.%, a significant (up to 16 mV) value of residual voltage after field treatment was found due to electromigration of Li ions. This phenomenon leads to a „reversed" type of hysteresis in the CVC dependences with respect to normal switching. In addition, the time dependences of the induced resistive states are extremely unstable in this case.

In structures M1/(CoFeB)$_x$(LiNbO$_3$)$_{100-x}$/s-LiNbO$_3$/M1, M3/(CoFeB)$_x$(LiNbO$_3$)$_{100-x}$/s-LiNbO$_3$/M3, containing boron, the magnitude of residual stress decreases due to the formation of chemical compounds of B atoms with percolated Li atoms. In the absence of electromigration processes of Li ions, the main mechanism of RP in these structures is associated with electromigration processes of oxygen vacancies in the dielectric oxide layer.

The suppression of residual stress in the M3/(CoFe)$_x$(LiNbO$_3$)$_{100-x}$/s-LiNbO$_3$/M3 structure by introducing a buffer layer of Cr, which does not dissolve Li, results in the absence of bipolar RP in these structures.

Conflict of interest

The authors declare that they have no conflict of interest.

References

[1] C. Li, M. Hu, Yu. Li, H. Jiang, N. Ge, E. Montgomery, Jm. Zhang, Wh. Song, N. Davila, C. Graves, Zh. Li, J. Strachan, P. Lin, Z. Wang, M. Barnell, Q. Wu, R. Williams, J. Yang, Qf. Xia. Nature Electr., **1**, 52 (2018). DOI: 10.1038/s41928-017-0002-z

[2] I.N. Antonov, A.I. Belov, A.N. Mikhaylov, O.A. Morozov, P.E. Ovchinnikov. J. Commun. Technol. Electron., **63** (8), 950 (2018). DOI: 10.1134/S106422691808003X

[3] A. Serb, J. Bill, A. Khiat, R. Berdan, R. Legenstein, T. Prodromakis. Nat. Commun., **7**, 12611 (2016) DOI: 10.1038/ncomms12611

[4] V.A. Demin, V.V. Erokhin, A.V. Emelyanov, S. Battistoni, G. Baldi, S. Iannotta, P.K. Kashkarov, M.V. Kovalchuk. Organic Electron., **25**, 16 (2015). DOI: 10.1016/j.orgel.2015.06.015

[5] A.V. Emelyanov, D.A. Lapkin, V.A. Demin, V.V. Erokhin, S. Battistoni, G. Baldi, A. Dimonte, A.N. Korovin, S. Iannotta, P.K. Kashkarov, M.V. Kovalchuk. AIP Advances, **6**, 111301 (2016). DOI: 10.1063/1.4966257

[6] K.E. Nikirui, A.V. Yemelyanov, V.V. Rylkov, A.V. Sitnikov, V.A. Demin. Pisma v ZhTF, **45** (8), 19 (2019) (in Russian).

[7] D. Ielmini. Semicond. Sci. Technol., **31**, 063002 (2016). DOI: 10.1088/0268-1242/31/6/063002

[8] J.S. Lee, S. Lee, T.W. Noh. Appl. Phys. Rev., **2** (3), 031303 (2015). DOI: 10.1063/1.4929512

[9] J.J. Yang, D.B. Strukov, D.R. Stewart. Nature Nanotech., **8**, 13 (2013). DOI: 10.1038/nnano.2012.240

[10] V.V. Rylkov, S.N. Nikolaev, V.A. Demin, A.V. Emelyanov, A.V. Sitnikov, K.E. Nikiruy, V.A. Levanov, M.Yu. Presnyakov, A.N. Taldenkov, A.L. Vasiliev, K.Yu. Chernoglazov, A.S. Vedeneev, Yu.E. Kalinin, A.B. Granovsky, V.V. Tugushev, A.S. Bugaev. J. Exp. Theor. Phys., **126**, 353 (2018). DOI: 10.1134/S1063776118020152

[11] V.A. Levanov, A.V. Emelyanov, V.A. Demin, K.E. Nikirui, A.V. Sitnikov, S.N. Nikolaev, A.S. Vedeneev, Yu.E. Kalinin, V.V. Rylkov. J. Commun. Technol. Electron., **63** (5), 491 (2018). DOI: 10.1134/S1064226918050078

[12] K.E. Nikiruy, A.V. Emelyanov, V.A. Demin, V.V. Rylkov, A.V. Sitnikov, P.K. Kashkarov. Tech. Phys. Lett., **44**, 416 (2018). DOI: 10.1134/S106378501805022X

[13] V.V. Rylkov, A.V. Sitnikov, S.N. Nikolaev, V.A. Demin, A.N. Taldenkov, M.Yu. Presnyakov, A.V. Emelyanov, A.L. Vasiliev, Yu.E. Kalinin, A.S. Bugaev, V.V. Tugushev, A.B. Granovsky. JMMM, **459**, 197 (2018). DOI: 10.1016/j.jmmm.2017.11.022

[14] V.V. Rylkov, S.N. Nikolaev, K.Y. Chernoglazov, V.A. Demin, M.Yu. Presnyakov, A.L. Vasiliev, V.V. Tugushev, A.B. Granovsky, A.V. Sitnikov, Yu.E. Kalinin, N.S. Perov, A.S. Vedeneev. Phys. Rev. B, **95** (14), 144202 (2017). DOI: 10.1103/PhysRevB.95.144202

[15] A.V. Sitnikov, I.V. Babkina, Y.E. Kalinin, A.E. Nikonov, M.N. Kopytin, A.R. Shakurov, O.I. Remizova, L.I. Yanchenko. ZhTF, **92** (9), 1382 (2022) (in Russian). DOI: 10.21883/JTF.2022.09.52930.94-22

[16] Yu.E. Kalinin, A.N. Remizov, A.V. Sitnikov. Phys. Solid State, **46** (11), 2146 (2004). DOI: 10.1134/1.1825563

[17] N. Domracheva, M. Caporali, E. Rentschler. *Novel Magnetic Nanostructures: Unique Properties and Applications* (Elsevier, 2018)

[18] I.A. Kedrinsky, V.G. Yakovlev. *Li-ion accumulators* (Platan, Krasnoyarsk, 2002)

[19] J. Rahn, E. Hüger, L. Dörrer, B. Ruprecht, P. Heitjans, H. Schmidt. Z. Phys. Chem., **226**, 439 (2012). DOI: 10.1524/zpch.2012.0214

[20] N.P. Lyakisheva. *Diagrammy sostoyaniya dvoynykh metallicheskikh sistem* (Mashinostroenie, M., 1997)

[21] R. Rupp, B. Caerts, A. Vantomme, J. Fransaer, A. Vlad. J. Phys. Chem. Lett., **10**, 5206 (2019). DOI: 10.1021/acs.jpclett.9b02014

[22] D.M. Gruen, A.R. Krauss, S. Susman, M. Venugopalan, M. Ron. J. Vac. Sci. Technol., **1** (2), 924 (1983). DOI: 10.1116/1.572152

Translated by Y.Deineka